Analysis of High Order Difference Methods for Multiscale Complex Compressible Flows

Björn Sjögreen[1] and H. C. Yee[2]

[1] Royal Institute of Technology, Sweden *bjorns@nada.kth.se*
[2] NASA Ames Research Center *yee@nas.nasa.gov*

1 Introduction

Accurate numerical simulations of complex multiscale compressible viscous flows, especially high speed turbulence combustion and acoustics, demand high order schemes with adaptive numerical dissipation controls. Standard high resolution shock-capturing methods are too dissipative to capture the small scales and/or long-time wave propagations without extreme grid refinements and small time steps. An integrated approach for the control of numerical dissipation in high order schemes with incremental studies was initiated in [15, 16, 9] and summarized in [17]. Here we further refine the analysis on, and improve the understanding of the adaptive numerical dissipation control strategy.

Basically, the development of these schemes focuses on high order nondissipative schemes and takes advantage of the progress that has been made for the last 30 years in numerical methods for conservation laws, such as techniques for imposing boundary conditions, techniques for stability at shock waves, and techniques for stable and accurate long-time integration. We concentrate on high order centered spatial discretizations and a fourth-order Runge-Kutta temporal discretizations as the base scheme. Near the boundaries, the base scheme has stable boundary difference operators [12]. To further enhance stability, the split form of the inviscid flux derivatives [5] is frequently used for smooth flow problems. To enhance nonlinear stability, linear high order numerical dissipations are employed away from discontinuities, and nonlinear filters are employed after each time step in order to suppress spurious oscillations near discontinuities to minimize the smearing of turbulent fluctuations.

Although these schemes are built from many components, each of which is well-known, it is not entirely obvious how the different components be best connected. For example, the nonlinear filter could instead have been built into the spatial discretization, so that it would have been activated at each stage in the Runge-Kutta time stepping. We could think of a mechanism that activates the split form of the equations only at some parts of the domain. Another issue is how to define good sensors for determining in which parts of the computational domain a certain feature should be filtered by the ap-

propriate numerical dissipation. For the present study we employ a wavelet technique introduced in [9] as sensors. Here, the method is briefly described with selected numerical experiments.

2 Base Schemes and Linear Numerical Dissipations

Consider a conservation law

$$u_t + f(u)_x = 0.$$

By a semi-discrete approximation

$$\frac{du_j(t)}{dt} + Df(u_j) = 0,$$

where D is a centered finite-difference operator, and $u_j(t)$ is the approximation of $u(x_j, t)$. A sixth-order spatial central operator

$$Du_j = (-u_{j-3} + 9u_{j-2} - 45u_{j-1} + 45u_{j+1} - 9u_{j+2} + u_{j+3})/(60\Delta x) \quad (1)$$

is used in our numerical examples. The resulting base scheme with a fourth-order Runge-Kutta in time is denoted by CEN66-RK4. Studies also were perform on the fourth and eighth-order centered schemes. The former is less accurate and the latter exhibits minor improvement and with a wider stencil and more complicated boundary operators over their sixth-order counterpart.

2.1 Boundary Operators

On the domain $j = 1, 2, \ldots, N$, the operator (1) traditionally applied at the points $j = 4, 5, \ldots, N-3$ with lower order centered and/or one-sided operators for $j = 2, 3$ and $j = N-2, N-1$. In order to have a stable initial-boundary value problem, non-traditional boundary operators that have the summation by parts (SBP) property are used. This means that in a weighted discrete scalar product,

$$(u, v)_h = \sum_{i=1,j=1}^{N,N} \sigma_{i,j} u_i v_j \Delta x$$

with $\sigma_{i,j}$ a positive definite matrix and $h = \Delta x$ the fixed grid spacing, we have the property

$$(u, Dv)_h = -(Du, v)_h + u_N v_N - u_1 v_1. \quad (2)$$

This implies that whenever stability can be obtained for the PDE by use of integration by parts, the same stability estimate can be made for the difference approximation by use of (2). Property 2 involved boundary operators

for grid points further away from the boundary than the traditional approach [12].

In the computations below we use boundary operators having the SBP property in a diagonal scalar product, and which are third-order accurate. Development of SBP operators was done by Kreiss in the 1970s. Later in [7], [12], the theory was revived and extended.

2.2 Entropy Splitting of the Inviscid Flux Derivatives

If the above conservation law can be symmetrized by a change of variables, $u = u(w)$, then

$$u(w)_t + f_w w_x = 0,$$

with $f_w = f_u u_w$ symmetric. If we furthermore assume that the flux function is homogeneous $f(\lambda w) = \lambda^\beta f(w)$, with $\beta \neq -1$, one can show that $\beta f = f_w w$. The thermally perfect gas dynamics have a family of variable transformations $u = u(w, \beta)$, defined by $w = E_u$, which give a homogeneous flux function. Here $E(u, \beta)$ is an entropy function of the conservation law.

Under the above assumption ($\beta < \frac{\gamma}{1-\gamma}$ or $\beta > 0$ for a perfect gas), the flux derivative can be split, resulting in the following form

$$u_t + \frac{\beta}{\beta+1} f_x + \frac{1}{\beta+1} f_w w_x = 0.$$

Taking the inner product with w, gives

$$-(\beta+1)(w, u_t) = \beta(w, f_x) + (w, f_w w_x) = \beta(w, f_x) + (f_w w, w_x).$$

Integration by parts in space and the homogeneity property $\beta f = f_w w$, give

$$(\beta+1)(w, u_t) = -[w^T f_w w]_a^b.$$

Homogeneity of the change of variables gives

$$\frac{d}{dt}(w, u_w w) = (\beta+1)(u_t, w) = -[w^T f_w w]_a^b. \tag{3}$$

Remark: The estimate (3) can be shown to be identical to

$$\frac{d}{dt} \int_a^b E(u)\, dx = [F]_a^b$$

obtained by integrating the entropy equation, $E_t + F_x = 0$, in space. Here F is the so called the entropy flux function.

It follows that $w u_w w = (\beta+1)E(u)$, see [13]. In [5] the entropy splitting is extended to conservation laws with nonhomogeneous flux functions. Formulas for symmetrizing the compressible Euler equations are given in [3]. Formulas

propriate numerical dissipation. For the present study we employ a wavelet technique introduced in [9] as sensors. Here, the method is briefly described with selected numerical experiments.

2 Base Schemes and Linear Numerical Dissipations

Consider a conservation law

$$u_t + f(u)_x = 0.$$

By a semi-discrete approximation

$$\frac{du_j(t)}{dt} + Df(u_j) = 0,$$

where D is a centered finite-difference operator, and $u_j(t)$ is the approximation of $u(x_j, t)$. A sixth-order spatial central operator

$$Du_j = (-u_{j-3} + 9u_{j-2} - 45u_{j-1} + 45u_{j+1} - 9u_{j+2} + u_{j+3})/(60\Delta x) \quad (1)$$

is used in our numerical examples. The resulting base scheme with a fourth-order Runge-Kutta in time is denoted by CEN66-RK4. Studies also were perform on the fourth and eighth-order centered schemes. The former is less accurate and the latter exhibits minor improvement and with a wider stencil and more complicated boundary operators over their sixth-order counterpart.

2.1 Boundary Operators

On the domain $j = 1, 2, \ldots, N$, the operator (1) traditionally applied at the points $j = 4, 5, \ldots, N-3$ with lower order centered and/or one-sided operators for $j = 2, 3$ and $j = N-2, N-1$. In order to have a stable initial-boundary value problem, non-traditional boundary operators that have the summation by parts (SBP) property are used. This means that in a weighted discrete scalar product,

$$(u, v)_h = \sum_{i=1,j=1}^{N,N} \sigma_{i,j} u_i v_j \Delta x$$

with $\sigma_{i,j}$ a positive definite matrix and $h = \Delta x$ the fixed grid spacing, we have the property

$$(u, Dv)_h = -(Du, v)_h + u_N v_N - u_1 v_1. \quad (2)$$

This implies that whenever stability can be obtained for the PDE by use of integration by parts, the same stability estimate can be made for the difference approximation by use of (2). Property 2 involved boundary operators

for entropy splitting of a perfect gas case are given in [2], and for a thermally perfect gas case are given in [16].

The above entropy splitting was used in a numerical method in [2], where the semi-discrete approximation was written as

$$\frac{du_j(t)}{dt} = -\frac{\beta}{\beta+1} Df(u_j) - \frac{1}{\beta+1} f_w(u_j) Dw_j. \tag{4}$$

Here, D is a difference operator, having the summation by parts property. Due to the SBP property, the relation

$$\frac{d}{dt}(w, u_w w)_h = -w_N^T f_w(w_N) w_N + w_1^T f_w(w_1) w_1 \tag{5}$$

in the discrete scalar product follows in the same way as was shown for the PDE. In the special case of periodic boundary conditions, the boundary terms disappear, and we conclude that the integrated entropy $(w, u_w w)_h$ is constant.

2.3 High Order Linear Numerical Dissipation/Filter

Numerical dissipation is normally needed in conjunction with entropy splitting. To minimize the lost of accuracy, we employ linear high order numerical dissipation obtained by adding an operator of the form

$$d(-1)^{q-1} \Delta x^{2q-1} (D_+ D_-)^q u_j$$

to the base scheme of order $q+2$ (or as a linear filter after the completion of the full step of the time discretization). Here d is a tunable parameter, and Δx is the grid spacing. The divided difference operators are defined by $D_+ u_j = (u_{j+1} - u_j)/\Delta x$, and $D_- u_j = D_+ u_{j-1}$. The dissipation operator has an order of accuracy $2q-1$, and dissipation of order $2q$. It is well known [6], [8], how to make a boundary modification to obtain an operator which is semi-bounded, i.e., which has the property

$$(-1)^{q-1} ((D_+ D_-)^q u_j, u_j)_h \leq 0. \tag{6}$$

If an extra stabilizing mechanism is desired for difference approximations on the split form, it is natural to define the dissipation on the entropy variables. The approximation (4) then becomes

$$\frac{du_j(t)}{dt} = -\frac{\beta}{\beta+1} Df(u_j) - \frac{1}{\beta+1} f_w(u_j) Dw_j + d(-1)^{q-1} \Delta x^{2q-1} (D_+ D_-)^q w_j. \tag{7}$$

If the SBP property and the semi-boundedness for the dissipation both hold in the same scalar product, we take the scalar product with w_j, and obtain as previously

$$\frac{d}{dt}(w, u_w w)_h = -w_N^T f_w(w_N) w_N + w_1^T f_w(w_1) w_1 - d||(D_+ D_-)^{q/2} w||_h^2. \quad (8)$$

The dissipation thus helps to control the increase of the entropy. An example where this applies is for periodic problems. For general boundary conditions, the dissipation has to be modified somewhat in order to obtain (8), because the scalar product for the summation by parts property is not the same as the standard scalar product used for the dissipation estimate. For the sixth-order base scheme, eighth-order linear dissipation ($q = 4$) is used and is denoted by CEN66-D8 without entropy splitting, and CEN66-ENT-D8 with the splitting.

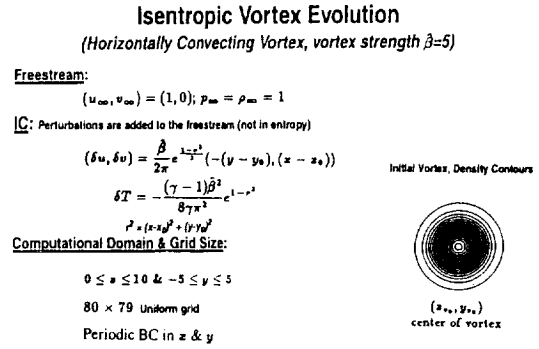

Fig. 1. Vortex convection problem description.

3 Long-Time Integration of Smooth Flows

Extensive numerical experiments on a 2-D compressible inviscid vortex convection with or without entropy splitting and/or nonlinear filter were conducted in [16, 9]. They showed that entropy splitting alone and/or nonlinear filter helps stabilize the scheme for a much longer convection time with almost perfect vortex preservation. Here we study the same problem for the behavior of the high order linear numerical dissipation and compare the solution with other well known methods. This is a pure convection problem and the exact solution should retain its shape. The problem is described in Fig. 1. The boundary conditions are periodic, and the solution is smooth, so that difficulties coming from boundary conditions and from non-smoothness of the solution are avoided. The computational domain is 10×10 with a uniform 80×80 grid. The time scale is such that one period corresponds to 10 time units. Density contours without entropy splitting and without any added dissipation (CEN66-RK4), are shown in Fig. 2. The solution after 5

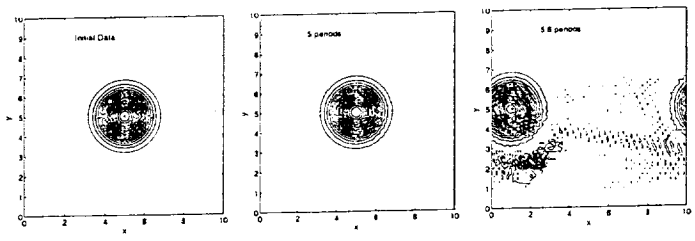

Fig. 2. Density contours after 0, 5, and 5.6 periods using CEN66-RK4.

periods has developed small, hardly visible, oscillations, and the computation breaks down before reaching 6 periods. The oscillations are due to nonlinear instabilities. Density contours using the entropy split form (4) (CEN44-ENT-

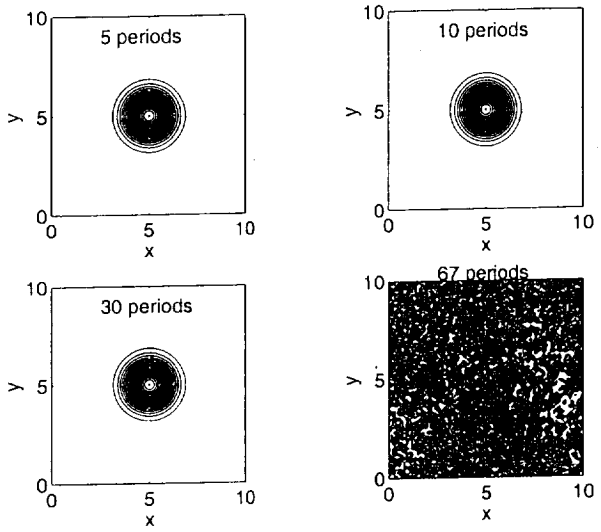

Fig. 3. Density contours using CEN66-ENT-RK4 with entropy split parameter, $\beta = 1$.

RK4) is shown in Fig. 3 with $\beta = 1$ (equal weight on the conservative and the non-conservative part). For this problem, $\beta = 1$ appears to be the best choice. Almost perfect vortex preservation is nearly 10 times longer than the unsplit case. However, the solution eventually breaks down (after 68 periods). For the entropy split method, it follows from (5) that the integrated entropy should be constant. Figure 4 shows the entropy integral as function of time for the computation in Fig. 3. The integrated entropy does decrease,

and the estimate holds, but is too weak. However, we have found that there are other values of β where the computed entropy integral increases. β does not appear in the semi-discrete estimate, but is apparently important for the time-discrete computations. It can be seen that entropy splitting retain the

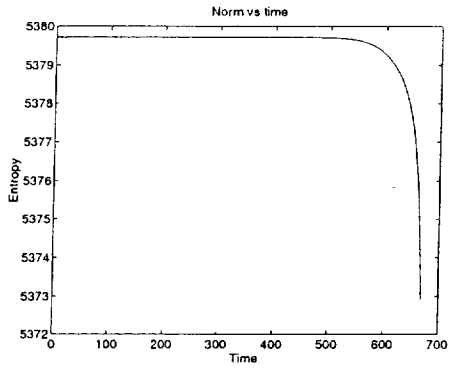

Fig. 4. Entropy integral vs. time of CEN66-ENT-RK4 with d =???, $\beta = 1$.

vortex shape from 5 periods to approximately 40 periods. However, in many applications, for example computation of rotorcraft flows, one needs to follow vortices for several hundred periods. We next investigate whether the use of high order linear numerical dissipation can be used to further increase the number of periods. Figure 5 shows the density contours of the sixth-order

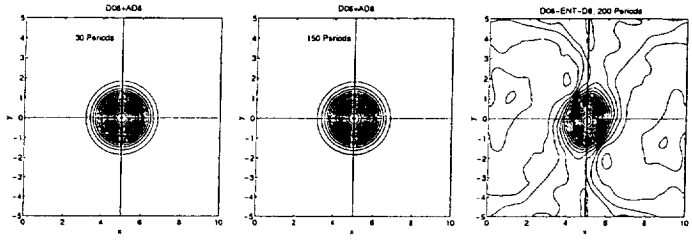

Fig. 5. Density contours by CEN66-D8-RK4 after 30, 150 and 200 periods.

base scheme with the eighth-order numerical dissipation added (CEN66-D8-RK4). The solution is very accurate up to approximately 150 periods, but the accuracy degenerates at later times. Although the accuracy becomes very poor, the solution did not break down. The computation could be run up to 300 periods, the maximum time we used. The coefficient d in front of the dissipation operator influences the behavior of the solution. The L^2 errors of

the solution as function of time for different values of the dissipation parameter d are shown in Fig. 6. The error norm is computed as the sum of the error norms of the four components. From Fig. 6, we conclude that there is an initial phase where the lower the dissipation, the better the accuracy, and the error increases in a "regular" way. At later times the larger dissipations have two points where the error increases quickly. For example, for $d = 8 \times 10^{-3}$ the first error increase comes at 70 periods and the second at 190 periods. We also conclude that for long-time integration, using the smallest possible dissipation is not optimal. After 120 periods the dissipation 1×10^{-3} gives a more accurate solution than the dissipation 5×10^{-4}. The smaller dissipation is insufficient to suppress the nonlinear instabilities. After 200 periods, all dissipations end up in a state where all accuracy is lost. The norm of the difference between the solution and the constant state with no vortex is approximately 0.1. Results using both entropy splitting and the linear nu-

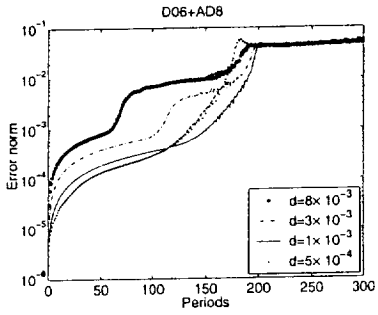

Fig. 6. Error vs. time for different dissipation coefficient d for CEN66-D8-RK4.

merical dissipation CEN66-ENT-D8 exhibit very minor improvement and no improvement at larger period of the vortex convection over the CEN66-D8 case. A possible explanation is that the very delicate cancellation properties, which keep the entropy split method stable, are destroyed by the numerical dissipation as time progresses. A fifth order WENO scheme (WENO5-RK4) [4], the so called DRP scheme [14], and a second-order accurate MUSCL TVD scheme (MUSCL-RK2) were computed for comparison. The WENO5 scheme is a general purpose scheme suited for flows with shock waves with no parameters to tune. The DRP scheme is designed for aeroacoustics. It is fourth-order accurate in space and second-order in time. Nonlinear instabilities are suppressed by a low order numerical dissipation term with a tunable parameter. We have tried to choose this dissipation strength as small as possible while keeping the scheme stable. Density contours are shown in Fig. 7 after 150 periods, and in Fig. 8 after 200 periods using the same contour levels. The MUSCL-RK2, and the DRP scheme are extremely diffusive. Both

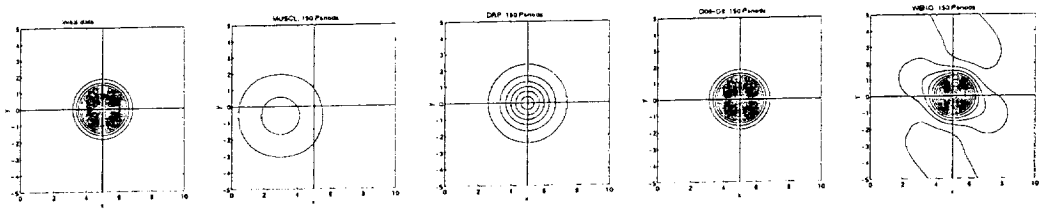

(a) IC (b) MUSCL (c) DRP (d) CEN66-D8 (e) WENO5

Fig. 7. Comparison of different methods: Density contours at 150 Periods

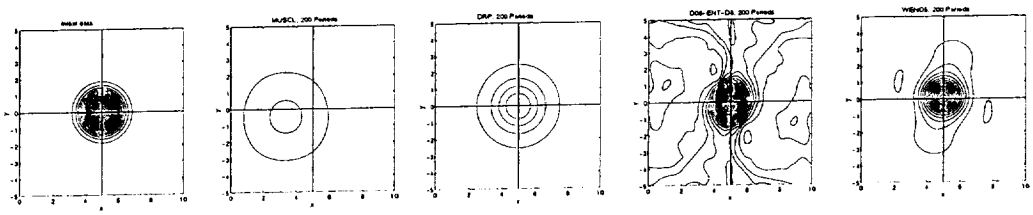

(a) IC (b) MUSCL (c) DRP (d) CEN66-D8 (e) WENO5

Fig. 8. Comparison of different methods: Density contours at 200 Periods

the WENO5 and the CEN66-D8 give better results. The error as function of time for the different methods is shown in Fig. 9. The error of MUSCL is not shown, instead the dashed curve shows the error of the entropy split sixth-order scheme, with $\beta = 1$, and no numerical dissipation (CEN66-ENT). After

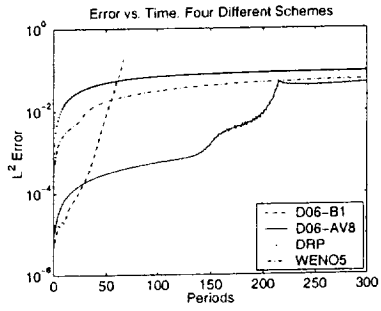

Fig. 9. Error vs. time for different methods.

200 periods, the result from the WENO5 scheme looks more pleasing to the eye, but as shown in Fig. 9, its error norm is larger than that of the centered scheme. The centered scheme loses accuracy due to dispersive errors, while for the other schemes, diffusive errors dominate. The performance of nonlinear filter scheme (including the use of the dissipative portion of WENO5 as a nonlinear filter) computations (same base scheme) are slightly more diffusive than CEN66-D8, and is reported in [9, 16, ?]. Studies on the blending of the linear dissipations with the nonlinear filters are reported in [17].

4 Nonlinear Filter/Numerical Dissipation for Discontinuities

The linear numerical dissipation used in the previous section is not strong enough to suppress the spurious oscillations due to the presence of shock and shear waves. A filter approach using nonlinear dissipation as a post processing filter, which is applied after each time step, is employed [15]. The filter consists of a conservative step

$$u_j^{n+1} = u_j^* - \lambda(h_{j+1/2}^* - h_{j-1/2}^*),$$

where u^* is the solution computed by the high order base scheme at time level $n+1$, and λ is the ratio of time step over Δx. For the numerical example the filter flux $h^*$is obtained from a second-order TVD scheme by subtracting the centered difference part and inserting a sensor, i.e.,

$$h_{j+1/2}^* = s_{j+1/2}(h_{j+1/2}^{TVD} - (f_{j+1} + f_j)/2).$$

The flux $h_{j+1/2}^{TVD}$ is the numerical flux of a second-order accurate TVD scheme. This TVD-flux typically contains flux limiters and Riemann solvers. The sensor $s_{j+1/2}$ is made such that the dissipation is switched on only near discontinuities. One example is to compute the local wavelet coefficients of the flow field by letting $s_{j+1/2}$ be close to unity where the wavelet coefficients show that the solution has poor regularity, and taking $s_{j+1/2}$ to be zero otherwise. See [9] for details. Computations using the dissipative portion of the WENO5 schemes or seventh-order high-resolution schemes were also considered. See [18] for an example using the WENO5 nonlinear dissipation.

5 2-D Shock/Shear/Boundary-Layer Interaction

Extensive grid refinement for shock-turbulence interactions, a complex multi-scale viscous combustion flows and a shock/shear/boundary-layer interaction are reported [17, 10, 11, 1]. Here we illustrate selected results for the complex shock/shear/boundary-layer interaction. An ideal gas is at rest in a 2-D box

$0 \leq x, y \leq 1$. A planar shock of Mach 2.37 located at $x = 1/2$ at time zero separates two different states of the gas. The 2-D compressible Navier-Stokes equation with no slip BCs at the adiabatic walls is used. The solution will develop complex 2-D shock/shear/boundary-layer interactions, which depend on the Reynolds number. The dimensionless initial states given in [1] are

$$\rho_L = 120, \quad p_L = 120/\gamma, \qquad \rho_R = 1.2, \quad p_R = 1.2/\gamma,$$

where ρ_L, p_L are the density and pressure respectively to the left of $x = 1/2$, and ρ_R, p_R are the same quantities to the right of $x = 1/2$. All velocities are equal to zero, $\gamma = 1.4$, the Prandtl number is 0.73, and the Reynolds number is 1000. All the computations stop at the dimensionless time 1 after the shock

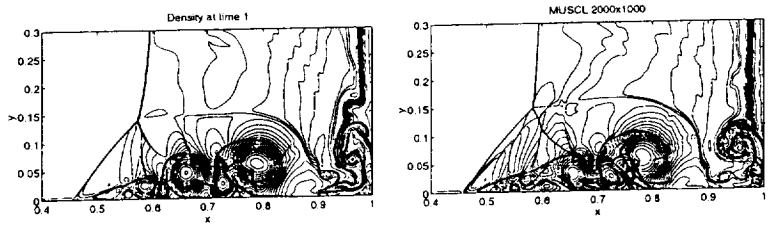

(a) 1000×500 grid (b) 2000×1000 grid

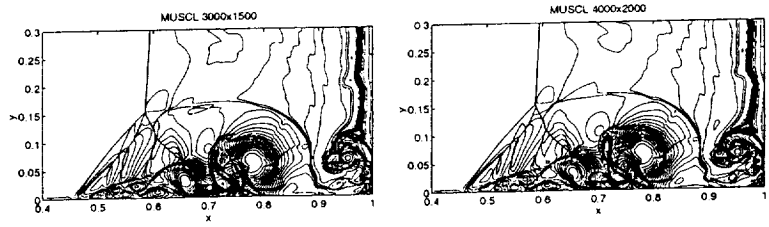

(c) 3000×1500 grid (d) 4000×2000 grid

Fig. 10. Grid refinement study: Density contours of MUSCL-RK2.

wave has reflected from the right wall and has almost reached the middle of the domain, $x = 1/2$. Due to the rapidly developing symmetry flow structure, a uniform Cartesian grid with the lower half of the domain is used. A grid convergence study of the sixth-order method with wavelet as the sensor to filter the solution using the nonlinear numerical dissipation (WAV66-RK4) is shown in Fig. 11. The same computation using the MUSCL-RK2 is shown in Fig. 10. Except for the largest vortical structure, the 1000×500 grid solution of WAV66-RK4 captures the overall flow structure of a 4000×2000 grid,

whereas the MUSCL scheme is still not convergent ever at a finer grid of 4000×2000. Since the filter is only applied once after each time step, the computational cost of WAV66-RK4 is almost the same as the computational cost of MUSCL-RK2 with the added advantage that the physical viscosities were taken into consideration by WAV66-RK4.

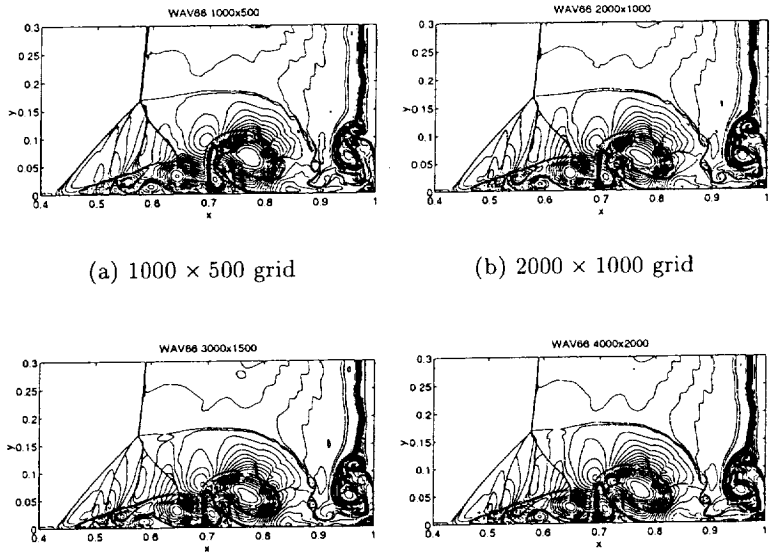

(a) 1000×500 grid (b) 2000×1000 grid

(c) 3000×1500 grid (d) 4000×2000 grid

Fig. 11. Grid refinement study: Density contours of WAV66-RK4.

References

1. V. Daru and C. Tenaud, *Evaluation of TVD High Resolution Schemes for Unsteady Viscous Shocked Flows*, Computers Fluids, **30** 89–113 (2000).
2. M. Gerritsen and P. Olsson, *Designing an Efficient Solution Strategy for Fluid Flows I.* J. Comput. Phys., **129** 245–262 (1996).
3. A. Harten, *On the Symmetric Form of Systems of Conservation Laws with Entropy*, J. Comput. Phys.,**49** (1983), pp. 151–164.
4. G.-S. Jiang and C.-W. Shu, *Efficient Implementation of Weighted ENO schemes*, ICASE Report No. 95-73, (1995).
5. P. Olsson and J. Oliger, J., *Energy and Maximum Norm Estimates for Nonlinear Conservation Laws*, RIACS Technical Report 94.01 (1994).
6. P. Olsson, *High-order Difference Methods and Data Parallel Implementation*, Doctoral Thesis, Department of Scientific Computing, Uppsala University, 1992.

7. P. Olsson, P., *Summation by Parts, Projections, and Stability. I*, Math. Comp. **64** 1035–1065 (1995).
8. B. Sjögreen, *High Order Centered Difference Methods for the Compressible Navier-Stokes Equations*, J. Comput. Phys., **117** 67–78 (1995).
9. B. Sjögreen and H. C. Yee, *Wavelet Based Adaptive Numerical Dissipation Control for Shock-Turbulence Computation*, RIACS Report 01.01, NASA Ames research center (Oct 2000).
10. B. Sjögreen and H. C. Yee, *Grid Convergence of High Order Methods for Multiscale Complex Unsteady Viscous Compressible Flows*, RIACS Report 01.06, April, 2001, NASA Ames research center; AIAA 2001-2599, Proceedings of the 15th AIAA CFD Conference, June 11-14, 2001, Anaheim, CA.
11. B. Sjögreen and H. C. Yee, *Low Dissipative High Order Numerical Simulations of Supersonic Reactive Flows*, RIACS Report 01-017, NASA Ames Research Center (May 2001); Proceedings of the ECCOMAS Computational Fluid Dynamics Conference 2001, Swansea, Wales, UK, September 4-7, 2001.
12. B. Strand, *Summation by Parts for Finite Difference Approximations for d/dx*, J. Comput. Phys. **110** 47–67 (1994).
13. E. Tadmor, *Skew-Selfadjoint Form for Systems of Conservation Laws*, J. Math. Anal. Appl., **103** 428–442 (1984).
14. C. K. W. Tam, *Computational Aeroacoustics: Issues and Methods*, AIAA journal, **33** (1995), pp. 1788–1796.
15. H.C. Yee, N.D. Sandham, N.D., and M.J. Djomehri, *Low Dissipative High Order Shock-Capturing Methods Using Characteristic-Based Filters*, J. Comput. Phys., **150** 199–238 (1999).
16. H.C. Yee, M. Vinokur, M., and M.J. Djomehri, *Entropy Splitting and Numerical Dissipation*, J. Comput. Phys., **162** 33-81 (2000).
17. H.C. Yee and B. Sjögreen, *Designing adaptive Low Dissipative High Order Schemes for Long-Time Integrations*, **Turbulent Flow Computation**, (Eds. D. Drikakis & B. Geurts), Kluwer Academic Publisher (2002); also RIACS Technical Report, Dec. 2001.
18. H.C. Yee and B. Sjögreen *Designing adaptive Low Dissipative High Order Schemes*, Proceedings of the ICCFD2, Sydney, Australia, July 15-19, 2002.